Journal of Power Sources 195 (2010) 3463–3471

Contents lists available at ScienceDirect

Journal of Power Sources

journal homepage: www.elsevier.com/locate/jpowsour

Characterization of interfacial morphology in polymer electrolyte fuel cells: Micro-porous layer and catalyst layer surfaces

F.E. Hizir[a], S.O. Ural[b], E.C. Kumbur[c], M.M. Mench[a,*]

[a] Fuel Cell Dynamics and Diagnostics Laboratory, Department of Mechanical and Nuclear Engineering, The Pennsylvania State University, University Park, PA 16802, USA
[b] Department of Materials Science and Engineering, The Pennsylvania State University, University Park, PA 16802, USA
[c] Department of Mechanical Engineering and Mechanics, 3141 Chestnut Street, Drexel University, Philadelphia, PA 19104, USA

ARTICLE INFO

Article history:
Received 5 October 2009
Received in revised form 6 November 2009
Accepted 9 November 2009
Available online 13 November 2009

Keywords:
Catalyst layer
Interface
Micro-porous layer
Polymer electrolyte fuel cell
Water management

ABSTRACT

The interface between the micro-porous layer (MPL) and the catalyst layer (CL) can have an impact on thermal, electrical and two-phase mass transport in a polymer electrolyte fuel cell (PEFC). However, there is scant information available regarding the true morphology of the MPL and CL surfaces. In this work, optical profilometry is used to characterize the MPL and CL surfaces at the sub-micron level scale to gain a better understanding of the surface morphology. Selected MPL and CL surfaces were sputtered with a thin layer of gold to enhance the surface reflectivity for improved data acquisition. The results show that, for the materials tested, the MPL surface has a relatively higher roughness than the CL surface, indicating the potential dominance of the MPL surface morphology on the local transport and interfacial contact across the MPL|CL interface. The level of roughness can be on the order of 10 μm peak height, which is significant in comparison to other length scales involved in transport, and can result in significant interfacial water storage capacity (approximately 6–18% of the total water content in a PEFC [37]) along this interface. Another surface characteristic that can have a profound influence on multi-phase transport is the existence of deep cracks along the MPL and CL surfaces. The cracks on MPL and CL surfaces are observed to differ significantly in terms of their orientation, size, shape, depth and density. The areal crack density of the CL tested is calculated to be $3.4 \pm 0.2\%$, while the areal crack density of the MPL is found to vary from 2.8% to 8.9%. The results of this study can be useful to understand the true nature of the interfacial transport in PEFCs.

1. Introduction

The growing interest in the usage of fuel cell power systems necessitates that the performance and durability be enhanced [1]. Some of the key factors that have critical importance are the surface conditions of various fuel cell components and the interactions between them [1–10]. Specifically, the interfacial characteristics of the micro-porous layer (MPL) and catalyst layer (CL), whose impact on the various polarization losses remains unknown, need further investigation.

Concentration polarization losses can be drastically influenced by the interfacial characteristics of fuel cell components and the gaps resulting from imperfect contact of the mating parts. In previous studies, the catalyst layer, gas diffusion layer (GDL) and flow channels were identified as possible locations of flooding [11]. Their impact on mass transport losses by blocking fuel and oxygen from reaching reaction sites were studied in detail. Effects of material and structural properties of the GDL and CL, such as their porosity, pore size, pore size distribution, tortuosity, thickness, and wettability, on water management-related issues were examined [11–17]. Recently, freeze/thaw studies performed at the Penn State Fuel Cell Dynamics and Diagnostics Laboratory have shown that interfacial gaps can exist between the MPL and CL following repeated cycling under certain extreme conditions [18–20]. Kim et al. [18] speculated on the role of these gaps as locations of water pooling, which could promote mass transport losses. Additionally, it has long been a matter of considerable speculation why certain manufacturers' MPL and GDL perform better with certain CL structures and worse with others. However, to date, the effects of MPL and CL surface topologies on the formation and characteristics of these interfacial gaps have not yet been quantitatively explored.

Surface roughness and topology of fuel cell components are influential on both thermal and electrical contact resistance losses, and this influence has been studied extensively by analyzing the bipolar plate (BPP) and GDL interface [2–7]. Surface treatments, which cause modifications in BPP surface characteristics, were shown to cause substantial changes in BPP|GDL interfacial contact resistance [2,3], and several modeling studies were conducted to predict the BPP|GDL interfacial contact resistance by taking the surface profiles of BPP and GDL into consideration [4–7]. However,

* Corresponding author. Tel.: +1 814 865 0060; fax: +1 814 863 4848.
E-mail address: mmm124@psu.edu (M.M. Mench).

0378-7753/$ – see front matter
doi:10.1016/j.jpowsour.2009.11.032

Nomenclature

R_a	average roughness (μm)
R_q	root mean square roughness (μm)
R_t	maximum height of the surface (μm)
R_p	maximum profile peak height (μm)
R_v	maximum profile valley depth (μm)
R_z	average maximum height of the profile (μm)
BPP	bipolar plate
CL	catalyst layer
GDL	gas diffusion layer
MPL	micro-porous layer
PEFC	polymer electrolyte fuel cell
SEM	scanning electron microscope
M	number of optical profilometry data points in the x-direction
N	number of optical profilometry data points in the y-direction
Z	surface height relative to the reference mean plane (μm)
H_j	distance between the jth highest peak and an arbitrary base plane (μm)
L_j	distance between the jth deepest valley and an arbitrary base plane (μm)
$Z_{max,peak}$	distance between the highest point of the surface and the reference mean plane (μm)
$Z_{min,valley}$	distance between the lowest point of the surface and the reference mean plane (μm)

little has been done to investigate the MPL|CL interfacial contact resistance, except a few experimental studies that were limited to measuring the bulk contact resistance rather than focusing on surface morphology of these layers [21,22]. To the best of the authors' knowledge, there is no work in the literature that examines the effects of MPL and CL surface topologies on the MPL|CL interfacial contact resistance either experimentally or computationally.

There exists a gap in the literature regarding how the MPL and CL surface morphologies, and the interfacial voids that occur between them, affect the various fuel cell polarization losses. This can be attributed to the experimental limitations involved in the three-dimensional characterization of the porous and highly irregular surfaces of the MPL and CL. In the reported studies, optical microscope, scanning electron microscope (SEM) and atomic force microscope (AFM) have been commonly employed to characterize the MPL and CL surface topography [22–24]. When compared, optical microscope measurements provide a relatively poor description of the MPL and CL surfaces due to relatively smaller depth of focus and limited resolution capabilities. Even though SEM imaging can provide a good overall view of the surfaces in two dimensions, it yields limited quantitative information regarding the height values of surface perturbations in the vertical direction. Moreover, direct acquisition of quantitative roughness values from two-dimensional SEM images is not possible. AFM can give three-dimensional data and quantitative roughness information compared to SEM. However, due to the highly rough nature of MPL and CL surfaces, the scanning area in AFM is limited to only few hundred square micrometers and the measurement speed is very small. A comparison of the imaging techniques commonly used to characterize surface topologies of fuel cell components is given in Table 1.

Optical profilometry is one viable solution to the measurement limitations imposed by AFM as it can acquire relatively large data sets in a reasonable amount of time. In addition to providing three-dimensional and quantitative measurements of surfaces with a vertical resolution on the order of several nanometers, optical profilometers are also capable of scanning areas as large as several hundred thousand square micrometers in less than a minute without having direct contact with the surface [25,26]. However, the major disadvantage of optical profilometry is its inability to scan light dispersive or poorly reflective surfaces. To achieve improved data acquisition, it is common practice to sputter poorly reflective surfaces with a thin layer of gold (Au) for enhanced reflectivity [25,27]. The gold layer thickness needs to be optimized to avoid introducing an artificial roughness to the surface by sputtering which can change surface structural properties [25,27–29].

Optical profilometry has been previously used to scan bipolar plate surfaces for which light reflectivity and dispersivity were not an issue [4]. Mishra et al. [4] used optical profilometry to scan the GDL surface that has low and irregular reflectivity patterns due to its fibrous and porous characteristics. Similarly, studies in pharmacology used optical profilometry together with gold sputtering to investigate the surface roughness characteristics of tablets. To ensure that the sputtering process did not induce any artificial roughness to the tablet surface; arbitrary regions on the surface were scanned with an SEM before and after gold sputtering, roughness parameters obtained from the SEM images were averaged and compared for closeness [27]. Characterization of wear damages in coatings [30], measurement of surface roughness of geosynthetic materials [31], quantification of changes in topographic structures of the skin [32] are some other applications that involve the use of optical profilometry for surface characterization.

This study is motivated by the need to have a quantitative understanding of the MPL and CL surface morphology at the submicron level, which will enable us to understand the true impact of the MPL|CL interfacial structure on performance of polymer electrolyte fuel cells (PEFCs). This is achieved by digitally characterizing the MPL and CL surfaces using optical profilometry. A special approach is designed to determine the optimum gold coating thickness required to perform optical profilometry measurements of the MPL and CL. Using SEM images and optical profilometry data of the sputtered MPL and CL samples, a detailed examination of the surface topography and roughness characteristics of the MPL and CL surfaces is performed. The approach presented in this work can be used to provide guidance for the future studies to investigate the effects of MPL and CL surface characteristics on mass transport and contact resistance losses.

2. Method of approach

Surfaces of the cracked catalyst layer and MPL of carbon felt type diffusion media (Sigracet gas diffusion layer, SGL 10BB series) were separately investigated. Material properties of SGL 10BB supplied by the manufacturer are given in Table 2. However, similar technical specifications of the cracked catalyst layer are not disclosed by the manufacturer.

To properly capture the surface topology of the samples by optical profilometry, surfaces of interest should possess a high degree of reflectivity. Since the CL and MPL possess low reflectivity and have light dispersive characteristics, the tested surfaces were sputtered with a thin layer of gold. The gold sputtering was performed in a Balzers SCD 050 Sputter Coater with a plasma current of 25 mA, at a working distance of 30 mm, and an Argon pressure of 30 Pa. Optical profilometry measurements were performed using a Wyko NT100 optical profilometer. In the measurements, the resolution in z-direction was approximately 3 nm, whereas the scanned area size was set to 604 μm × 459 μm with a sampling interval of 0.82 μm in the x-direction and 0.95 μm in the y-direction.

Table 1
Comparison of the tools commonly employed for the surface characterization of fuel cell components.

Method	Quantitative information	3D data	Resolution (nm)		Limitation(s)	Advantage(s)
			Horizontal	Vertical		
Optical microscope	No	No	30–1000	–	Limited resolution. Small depth of focus. Only a 2D view of the surface.	Fast and inexpensive. Applicable to a variety of samples of any roughness.
Stylus profilometer	Yes	Yes	15–100	0.1–1	Surface deformation of the sample. Slow measurement speed in 3D mapping. Inability to measure deep grooves and vertical surfaces.	
Scanning electron microscope	Limited	Yes[a]	≈5	10–50	Direct acquisition of quantitative roughness values not possible. Applicable to conductive surfaces and vacuum compatible samples. Risk of burning and melting of heat sensitive materials.	Good overall view of the sample. More flexibility in sample surface orientation compared to AFM. Much better resolution, contrast, and depth of focus compared to optical microscope.
Atomic force microscope	Yes	Yes	0.2–1	≈0.02	Small scanning area. Slow measurement speed. Difficulties in scanning rough surfaces.	High resolution measurements. No surface damage when operated in non-contact mode.
Optical profilometer	Yes	Yes	500–5000	3–10	Inability to scan poorly reflective or light dispersive surfaces. Inability to measure deep grooves and vertical surfaces.	Non-contact and damage-free measurements. High resolution measurements. A good and broad overall view of the surface provided in a reasonable time.

[a] With special techniques only, normal SEM images are not three-dimensional.

2.1. Determination of optimum sputtering time for optical profilometry measurements

Special sputtering protocols were developed for the tested CL and MPL surfaces to determine the optimal sputtering time for improved profilometry measurements. For the catalyst layer, six different CL samples were sputtered with Au for 40 s, 1 min, 2 min, 3 min, 4 min and 6 min, respectively. Arbitrary areas were scanned on each sample, and two-dimensional optical profilometry images of the scanned areas were captured for further analysis (Fig. 1a). The number of black points on the images (missing data points due to low reflectivity or physical pores in the surface) was observed to dramatically decrease with increasing sputtering time up to 4 min. For sputtering times longer than 4 min, a significant improvement in optical profilometry images was not observed, indicating that 4 min of sputtering is sufficient to acquire the necessary set of surface scan data for the tested CL surface. It should be noted that after 4 min of sputtering, the vast majority of black data points represents the surface pores of the tested CL samples.

Once the critical sputtering time was determined, the effects of increasing gold coating thickness on the surface morphology of the CL were investigated. This was accomplished by post-mortem SEM image analysis. Initially, the SEM images of a specific region on a virgin CL specimen were captured without any sputtering by using a Hitachi S-3000H scanning electron microscope. Then the SEM images of the same region were captured after the sputtering of the same sample for 2 min, 3 min and 4 min via the application of a series of sequential sputtering processes. The captured SEM images indicated a small growth in surface particle size (on the order of 0.01 μm) and a small decrease in surface pore size (on the order of 0.01 μm) for 4 min sputtering case (Fig. 2a). This suggests that 4 min of sputtering does not significantly change the surface morphology of CL samples. Therefore, for the material tested, optical profilometry measurements can be conveniently performed on a 4 min sputtered CL sample.

The sputtering operations performed during the optical profilometry analysis take place in a single step, while those performed during the SEM analysis take place in multiple steps. However, this is not expected to change the total thickness of the gold layer and its distribution over the sample surface for the same total sputtering time. Hence, the optical profilometry images and the corresponding SEM images can still be coupled and compared to draw conclusions on the optimum sputtering time. Additionally, the coincidence of the SEM images for different durations of Au-sputtering, confirms that the apparent high porosity (large number of black spots) in optical profilometry images of the thinly sputtered samples is due to low reflectivity and that its apparent reduction at higher sputtering times is due to a more accurate picture rather than filling of the pores by deposited Au.

A similar procedure used for CL samples was employed to determine the optimal sputtering time for the MPL. Optical profilometry images of arbitrary points on five different MPL samples: a non-sputtered sample and samples sputtered for 4 min, 5 min, 6 min, and 7 min were captured (Fig. 1b). Data regarding crack depth and profile could not be completely determined, no mat-

Table 2
Material properties of SGL 10BB [45].

Properties	Value	Unit
Thickness	420	μm
Areal weight	125	$g\,m^{-2}$
Porosity	84	%
Air permeability	3	$cm^3\,cm^{-2}\,s$
Electrical resistance (through plane)	<15	$m\Omega\,cm^2$
Existence of MPL	Yes	

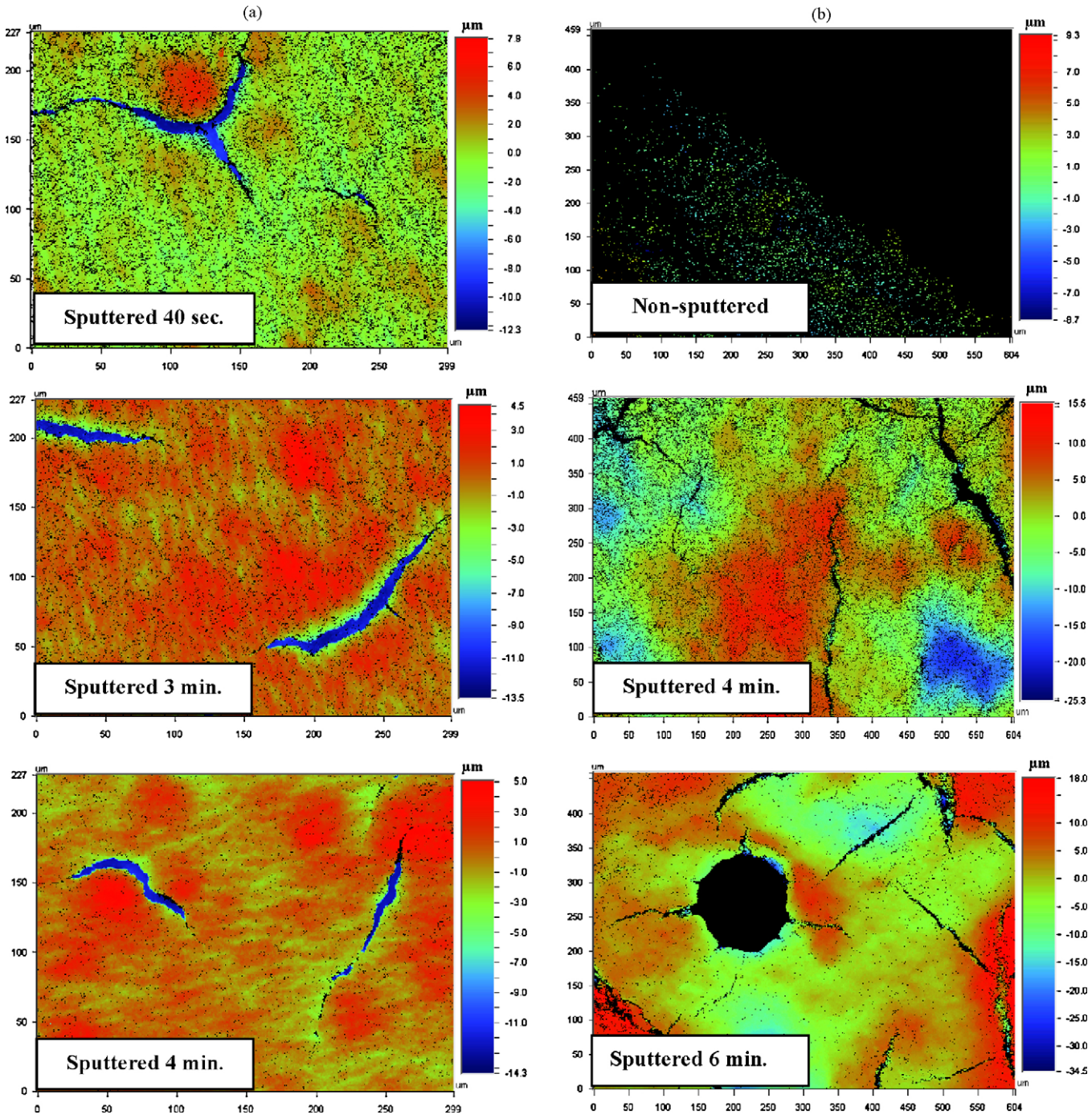

Fig. 1. (a) Two-dimensional optical profilometry images of naturally cracked catalyst layer. (b) Two-dimensional optical profilometry images of MPL side of SGL 10BB.

ter how much sputtering is applied on the surface. However, missing data from the remaining portions of the surface were observed to decrease with increasing sputtering time, as expected. Comparing the images, 6 min of sputtering was concluded to be sufficient to get satisfactory optical profilometry data from the type of MPL tested (SGL 10BB). Afterwards, SEM images of the exact same region on a single MPL sample were captured for a virgin case and several sputtered cases (*i.e.* 4 min, 5 min, 6 min and 11 min). For sputtering times up to 6 min, no changes in the SEM images were observed compared to the non-sputtered case, leading to the conclusion that 6 min of sputtering would provide sufficient resolution to perform profilometry measurements of the MPL. On the other hand, excessive sputtering times, such as 11 min, were observed to alter the surface morphology of MPL significantly, *e.g.* causing a 0.5 μm growth in particle size and leading to a significant decrease in surface porosity, as shown in Fig. 2b.

2.2. Optical profilometry measurements and roughness analysis

Optical profilometry measurements were performed for 18 different locations on MPL and cracked CL surfaces after applying 6 min and 4 min of sputtering, respectively. Measurement locations were selected to be distributed uniformly over the surfaces at evenly spaced locations. Variation of height as a function of x and y coordinates was obtained for each scanned region. The data sets

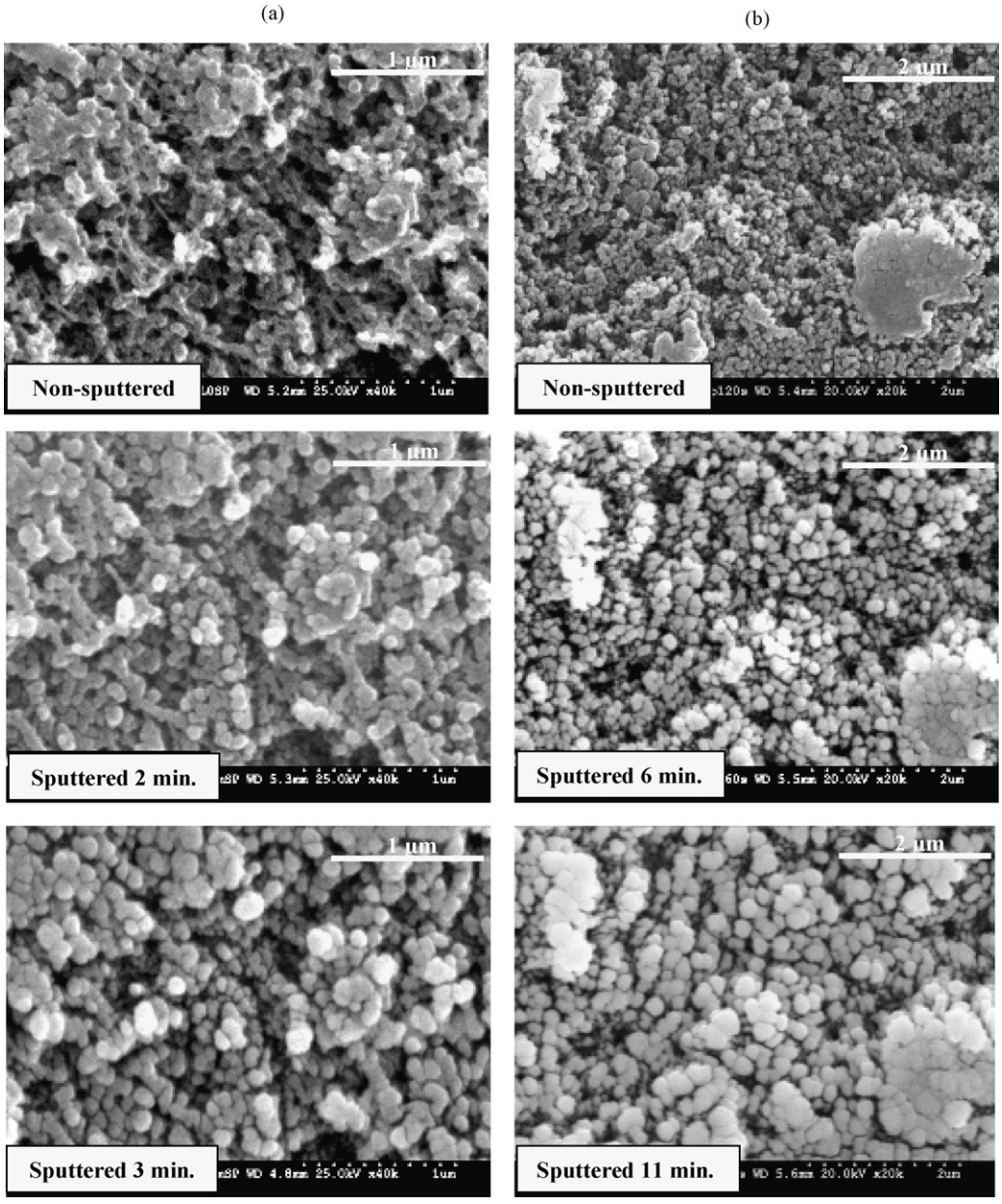

Fig. 2. (a) SEM images of naturally cracked catalyst layer. (b) SEM images of MPL side of SGL 10BB.

obtained were later used to calculate the amplitude parameters of the scanned regions for roughness analysis.

2.3. Analysis of SEM images and crack density calculations

To have a better understanding of the surface characteristics of the samples, additional SEM images of virgin MPL and cracked CL surfaces were captured at higher working distances. SEM images were analyzed with the open source software ImageJ [33] for crack density calculations, after being edited for visual clarity on Adobe Photoshop. Boundaries of the cracks were sharpened using a brush of size one pixel. The dust particles within the non-cracked regions and fiber fragments trapped in the cracked regions were eliminated. Any non-uniformities in color within the cracks were converted to black so that the regions inside and outside the cracks could contrast sharply when the SEM images were converted to binary form. An automatic thresholding algorithm of ImageJ was used to convert the original gray scale SEM images to binary form. Crack density values were calculated by taking the ratio of number of black pixels to the total number of pixels for 10 different SEM images of MPL and CL, and averaging the results.

3. Results and discussion

3.1. MPL and CL surface characteristics

Optical profilometry results indicate that both MPL and cracked CL surfaces exhibit a relatively high degree of roughness, having perturbations in the form of high hills, large valleys and deep cracks on the surface (Figs. 3 and 4). To characterize and compare the morphologies of different surfaces, various parameters describing surface characteristics can be used [27,34,35]. In this study, amplitude parameters determined via using the optical profilometry data were analyzed and utilized to compare the morphologies of MPL and CL surfaces. Since the use of a single amplitude parameter can lead to dubious conclusions [26], a set of six amplitude parameters

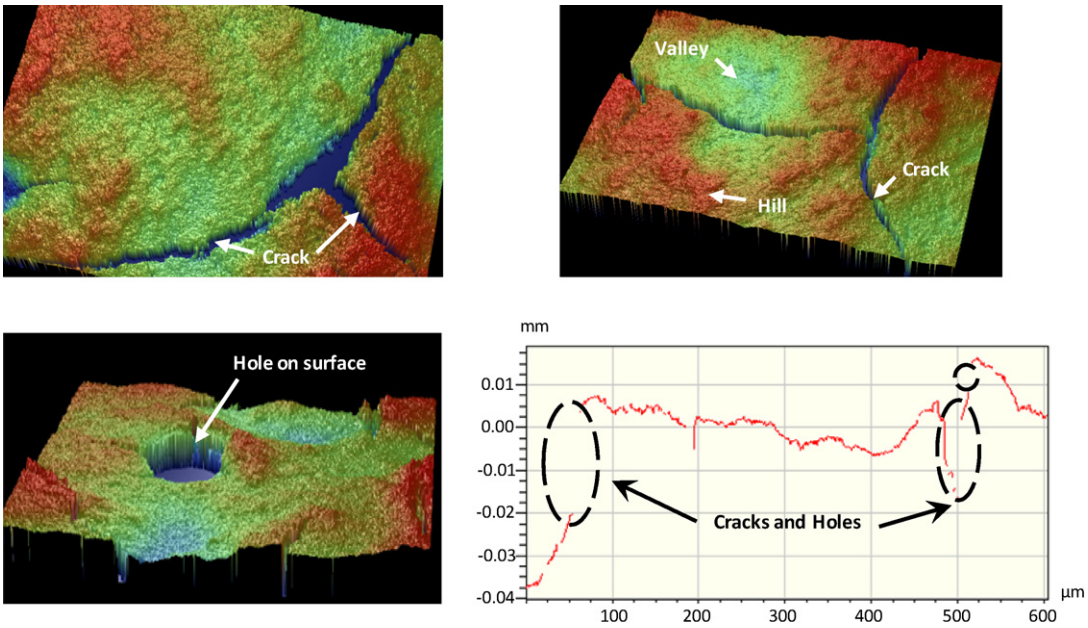

Fig. 3. Representative three-dimensional images and surface profile of MPL of SGL 10BB obtained using optical profilometry.

(average roughness (R_a), root mean square roughness (R_q), average maximum height of the profile (R_z), maximum profile peak height (R_p), maximum profile valley depth (R_v), maximum height of the surface (R_t)) were used to compare surface roughness of MPL and CL surfaces. The reader can refer to British Standards [36] for a detailed description of the amplitude parameters, which are summarized in Table 3. Amplitude parameters of the MPL surface are found to be higher than the amplitude parameters of the CL surface (Tables 4 and 5), which indicates that the MPL surface exhibits a higher degree of roughness than the cracked CL surface for the materials tested.

SEM images show that there are significant differences between the cracks on the MPL and CL surfaces in terms of their orientation, size, shape, depth and density (Fig. 5). Cracks on this type of CL surface are in the shape of thin ribbons that are aligned with respect to each other. There is no significant variance in the crack width, which is around 15 µm at the crack center. The SEM images and the height values in the profilometry data indicate that cracks can

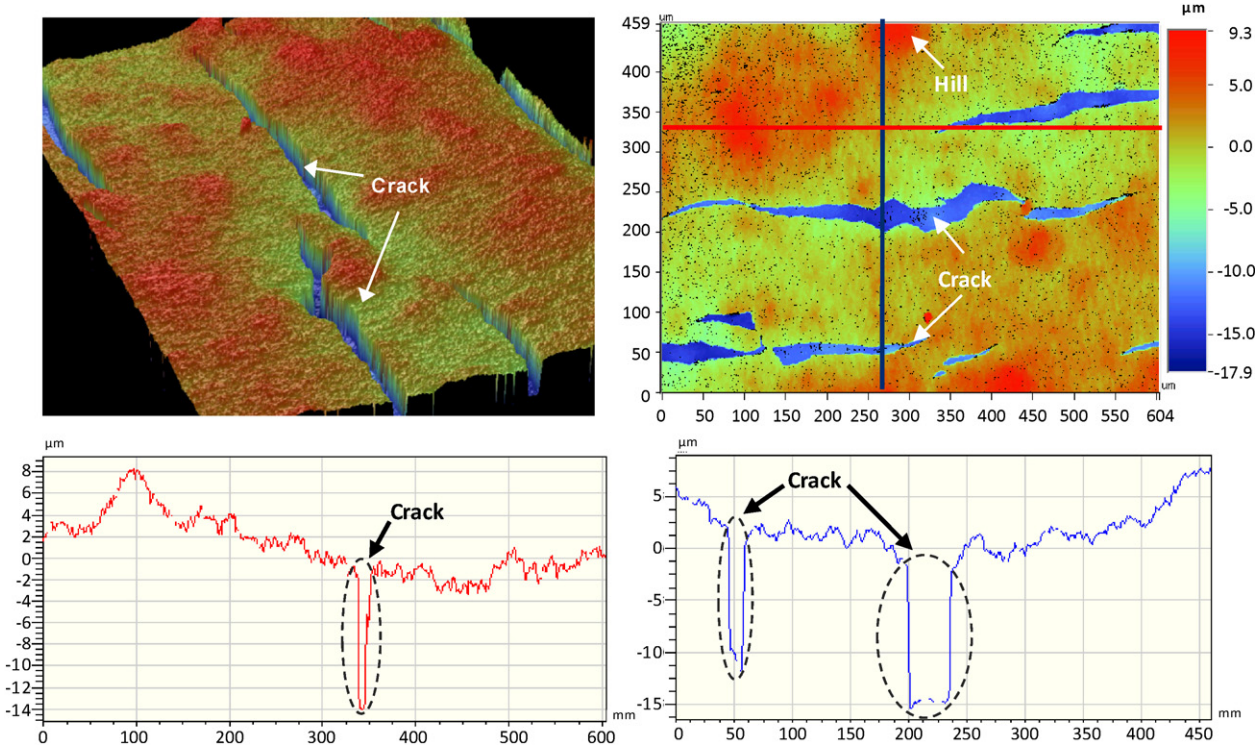

Fig. 4. Representative three-dimensional image, two-dimensional image, surface profile in X-direction (along the red line), and surface profile in *y*-direction (along the blue line) of cracked catalyst layer obtained using optical profilometry. (For interpretation of the references to color in this figure legend, the reader is referred to the web version of the article.)

Table 3
Definitions of amplitude parameters [36].

Parameter	Description	Formula
R_a	Average roughness	$\frac{1}{MN}\sum_{j=1}^{M}\sum_{i=1}^{N}\left\|Z_{ij}\right\|$
R_q	Root mean square roughness	$\sqrt{\frac{1}{MN}\sum_{j=1}^{M}\sum_{i=1}^{N}\left\|Z_{ij}^2\right\|}$
R_z	Average maximum height of the profile	$\frac{1}{10}\left[\sum_{j=1}^{10}H_j-\sum_{j=1}^{10}L_j\right]$
R_p	Maximum profile peak height	$Z_{\max,peak}$
R_v	Maximum profile valley depth	$Z_{\max,depth}$
R_t	Maximum height of the surface	$Z_{\max,peak}+\left\|Z_{\max,depth}\right\|$

Table 4
Measured amplitude parameters for each of the 18 points scanned on the MPL (SGL 10BB) surface (last line indicates mean values ± standard deviation of 18 measurements).

Point	R_a (μm)	R_q (μm)	R_t (μm)	R_z (μm)	R_p (μm)	R_v (μm)
1	2.00	3.36	22.86	22.05	7.09	−15.77
2	2.16	3.60	27.24	25.50	9.31	−17.93
3	2.08	3.60	25.99	24.93	9.21	−16.78
4	2.16	3.60	28.23	27.09	11.74	−16.48
5	2.16	3.68	21.81	21.36	6.61	−15.20
6	1.92	3.44	22.84	21.97	6.78	−16.06
7	2.64	4.08	26.45	25.35	10.32	−16.13
8	2.16	3.52	27.54	26.07	10.49	−17.06
9	2.32	3.60	22.63	22.10	6.37	−16.26
10	2.24	3.76	26.67	23.95	8.78	−17.89
11	2.24	3.68	26.68	23.49	10.31	−16.37
12	2.00	3.52	27.88	27.12	11.30	−16.58
13	1.92	3.36	27.39	23.65	7.61	−19.78
14	2.08	3.60	26.33	25.03	8.86	−17.47
15	2.32	3.84	34.28	26.75	12.21	−22.07
16	2.08	3.44	24.72	23.31	7.35	−17.37
17	2.64	4.08	25.95	24.71	8.83	−17.12
18	2.24	3.60	32.62	28.77	15.34	−17.28
	5.35 ± 1.96	7.39 ± 3.20	68.32 ± 19.95	63.50 ± 20.34	18.04 ± 3.17	−50.28 ± 19.37

extend through the entire CL thickness, having an average crack density of 3.4 ± 0.2%. On the contrary, cracks on the MPL surface are randomly oriented with larger and variable width which can be as large as 60 μm. Holes and dents with diameter on the order of 100 μm are also present on the MPL surface. These frequent and relatively large cracks could conceivably play an important role in the multi-phase flow along and through the interfaces, a topic that is in need of great study. The frequency of these holes on the MPL surface is not constant, showing variation from one location to another. In some regions, these holes/dents are observed to be very closely located, whereas they are very rare or not present in some other regions. Depending on the frequency of these holes, the areal crack

Table 5
Measured amplitude parameters for each of the 18 points scanned on the CL surface (last line indicates mean values ± standard deviation of 18 measurements).

Point	R_a (μm)	R_q (μm)	R_t (μm)	R_z (μm)	R_p (μm)	R_v (μm)
1	5.68	6.88	57.96	55.22	16.70	−41.26
2	5.84	6.80	54.94	45.22	18.52	−36.43
3	4.40	6.88	91.72	81.65	19.33	−72.39
4	4.40	6.88	91.72	86.72	19.33	−72.39
5	4.32	5.36	55.78	51.06	20.85	−34.93
6	3.84	4.64	50.54	48.45	13.39	−37.16
7	4.80	6.16	52.43	48.08	17.96	−34.47
8	3.92	6.08	85.94	77.38	16.36	−69.58
9	8.88	13.44	88.97	86.60	16.45	−72.51
10	3.60	4.40	45.27	39.33	12.49	−32.79
11	7.84	12.24	100.82	95.19	19.35	−81.46
12	4.08	5.12	52.49	47.79	21.02	−31.47
13	5.76	7.36	64.02	60.88	20.35	−43.67
14	4.64	5.92	52.38	44.79	22.20	−30.18
15	3.76	6.32	67.63	66.02	13.81	−53.83
16	6.56	8.24	67.13	65.71	22.78	−44.34
17	3.52	4.48	45.63	39.17	13.50	−32.13
18	10.48	15.84	104.39	103.74	20.29	−84.10
	2.19 ± 0.20	3.63 ± 0.21	26.56 ± 3.19	24.62 ± 2.07	9.36 ± 2.34	−17.20 ± 1.58

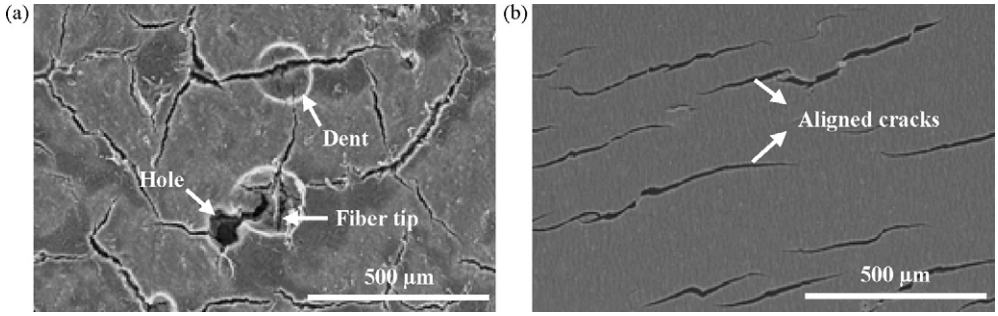

Fig. 5. (a) Representative SEM image of MPL side of SGL 10BB. (b) Representative SEM images of cracked CL.

density was found to vary from 2.8% to 8.9%. Although optical profilometry data regarding crack depth is missing, the data obtained from few points on the crack base indicate that the crack depth can be as large as the MPL thickness. This can be observed in the captured SEM images, where the fibers belonging to the GDL can be visible through some of the cracks on the MPL surface. These observations form strong evidence that a certain portion of the cracks on the MPL surface can extend through the entire MPL thickness, reaching to the GDL|MPL interface.

3.2. Implications of the results

Due to the rough and cracked nature of the MPL and CL surfaces, the contact between these two layers will be imperfect under compression. This imperfect contact may result in the formation of interfacial gaps with uneven compression pressure between the MPL and CL surfaces and consequently a reduction in contact area (Fig. 6). The reduced contact area may interfere with the flow of electrons across the MPL|CL interface and cause an increase in the MPL|CL electronic contact resistance. In addition, due to the absence of electrochemical reactions and heat generation in the interfacial gaps, thermal disruptions may be generated, which will impact multi-phase flow as well. Uneven compression from the MPL to CL surfaces can also result in reduced durability.

The interfacial gaps at the MPL|CL interface (especially, where cracked and non-cracked spots come up against each other) may also act as water accumulation sites (pooling locations) and prevent the reactant gases from reaching active sites in the CL. As the peak height and crack depth of the MPL and CL are on the same order of magnitude as their thickness, the volume of the interfacial gaps at the MPL|CL interface are expected to be comparable to the total pore volume of the MPL and CL. This suggests that the interfacial gaps at the MPL|CL interface could have a large water storage capacity and consequently a strong impact on the mass transport losses. In support of this prediction, Swamy et al. [37] argued that the MPL|CL interface could hold approximately 6–18% of the total water content in a PEFC when filled, which is significant amount of water when the overall water balance in PEFCs is considered. Moreover, in sub-freezing environments, water in the interfacial gaps may result in ice lens formation and growth between the MPL and CL. With repeated freeze/thaw cycles, this may lead to interfacial delamination between the GDL and CL, permanent deformation of the GDL and fracturing of its carbon fibers resulting in reduced longevity and operational stability. As MPL surface is rougher than the CL surface, tailoring the MPL surface for better mating characteristics could be beneficial for reducing the losses and degradation associated with the interface.

In a vast majority of modeling studies, the MPL was considered to be a purely homogenous porous medium, and the effects of incomplete contact, macro-cracks and holes in the MPL structure were not taken into account. Although the MPL is typically considered to act as a capillary barrier that directs liquid flow from cathode to anode [38,39], the macro-cracks and holes in the MPL structure may act as water transport channels that carry the liquid water from cathode CL to the cathode GDL|MPL interface (Fig. 7). Gostick et al. [40] argued that cracks in the MPL could be beneficial, as they have the potential to reduce the GDL saturation by limiting the number of dead-end clusters formed in the GDL. They suggested that water entry into the GDL takes place mainly through the cracks on the MPL surface. Hence, the pores on the remaining portions of the GDL face (where there is no overlap with the cracks on the MPL face) remain inaccessible to water and form paths for gas-phase reactant transport.

Interfacial gaps at the MPL|CL interface may also impose different roles on the MPL cracks, depending on the operating current density. Under low current density operating conditions, MPL cracks may serve to evacuate the liquid water that tends to accumulate inside the MPL|CL interface, and keep the interfacial gaps dry for gas-phase reactant transport. However, under high current density operating conditions, the amount of water generated in the CL may exceed the water storage capacity of the MPL cracks, and the interfacial gaps may start to fill with liquid water. In this case, the liquid-filled MPL cracks may promote flooding at the MPL|CL interface.

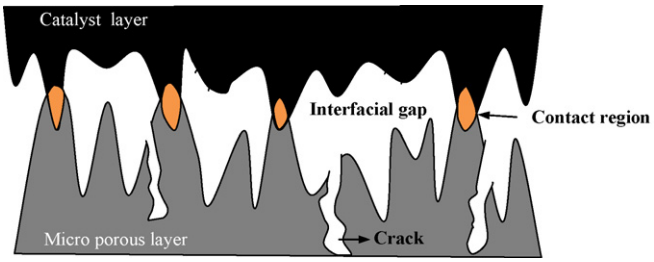

Fig. 6. Two-dimensional schematic of the MPL|CL interfacial contact.

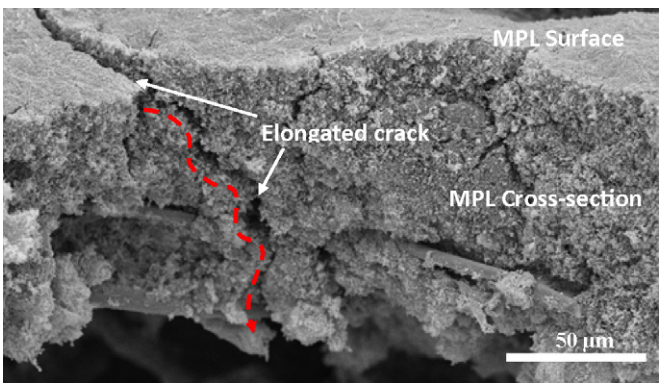

Fig. 7. Cross-sectional SEM image of MPL of SGL 10BB (arrow indicates the flow path formed by the cracks).

Furthermore, cracks in the MPL could alter the saturation and water mass distribution in the MPL substantially by holding a significant amount of water. Approximating the crack depth to be as large as the MPL thickness for all the cracks in the MPL and the MPL thickness to be 80 μm, the MPL cracks can hold 0.22 mg cm^{-2} to 0.71 mg cm^{-2} of water when fully filled for the calculated areal crack density of the MPL. In his recent neutron imaging work, Turhan et al. [41] observed a reversed saturation profile at the MPL|GDL interface with the MPL having a higher level of effective total saturation than the GDL, in contrast to the modeling studies that predict a higher level of GDL saturation for similar conditions. In addition to phase-change-induced flow, this unexpected increase in the MPL water saturation can be explained by the liquid water held by the MPL cracks. Cross-sectional X-ray radiography results [42] indicating the existence of significant water accumulation around the MPL|CL and MPL|GDL interfaces may also be attributed to the wide MPL cracks that are filled with liquid water. Similarly, Nam et al. [43] claimed that size of the pores on the MPL surface control the interfacial saturation and size of the droplets formed at the MPL|CL interface, supporting the theory that MPL cracks could promote droplet growth, coalescence and accumulation.

Cracks on the CL surface are expected to have significant impact on fuel cell performance, as well. Removal of the platinum on the CL surface due to cracking may result in the formation of platinum-deficient sites and a reduction in the electrochemically active area. The study by Manahan et al. [44] reports higher activation polarization losses for CL with high cracking compared to CL with negligible cracking, which is in good agreement with our hypothesis.

4. Conclusions

In this study, optical profilometry and SEM were used to characterize the surfaces of the MPL and CL. The results show that both the MPL and CL possess relatively rough surface characteristics, which could lead to the formation of significant interfacial gaps at the MPL|CL interface due to imperfect contact. As the peak height and valley depth of the MPL and CL surfaces are comparable to their thickness, the interfacial gaps are expected to have significant water storage capacity and impact on mass transport losses under compression. More importantly, formation of ice lenses due to freezing of the water stored in the interfacial gaps at sub-freezing temperatures is expected to result in accelerated degradation of the MEA and GDL. The MPL surface is found to exhibit a higher degree of roughness compared to the CL surface, suggesting that tailoring the MPL surface for improved interface mating characteristics could reduce interfacial losses and membrane durability. Another observation is the existence of cracks in the MPL and CL structures, cracks in the MPL being relatively wider and deeper. MPL cracks are expected to cause an increase in the water held by the MPL, and affect the saturation behavior at the MPL|GDL and MPL|CL interfaces. Additionally, cracks in the MPL may act as water transport channels, helping to explain the discrepancies between modeling predictions and observed water saturation profiles. The results of this study can be used in further investigations to understand the impact of the interfacial morphology and surface cracks on multiphase flow, and interfacial electronic and thermal resistances at the MPL|CL interface.

Further investigations are underway at the PSU FCDDL to understand the effects of the MPL and CL cracks on fuel cell performance, and to improve the contact between MPL and CL surfaces for reduced interfacial losses.

Acknowledgements

This work was supported by the Toyota Motor Corporation, Japan. M.M. Mench thanks NSF CAREER award #0644811 for partial support. Mr. A.K. Heller' s support to measure the surface crack density using ImageJ is greatly appreciated.

References

[1] M.M. Mench, Fuel Cell Engines, John Wiley & Sons, Inc., Hoboken, NJ, 2008.
[2] B. Avasarala, P. Haldar, J. Power Sources 188 (2009) 225–229.
[3] A. Kraytsberg, M. Auinat, Y. Ein-Eli, J. Power Sources 164 (2007) 697–703.
[4] V. Mishra, F. Yang, R. Pitchumani, J. Fuel Cell Sci. Technol. 1 (2004) 2–9.
[5] Y. Zhou, G. Lin, A.J. Shih, S.J. Hu, J. Power Sources 163 (2007) 777–783.
[6] Z. Wu, Y. Zhou, G. Lin, S. Wang, S.J. Hu, J. Power Sources 182 (2008) 265–269.
[7] Z. Wu, S. Wang, L. Zhang, S.J. Hu, J. Power Sources 189 (2009) 1066–1073.
[8] X. Lai, D.A. Liu, L. Peng, J. Ni, J. Power Sources 182 (2008) 153–159.
[9] L. Zhang, Y. Liu, H. Song, S. Wang, Y. Zhou, S.J. Hu, J. Power Sources 162 (2006) 1165–1171.
[10] I. Nitta, T. Hottinen, O. Himanen, M. Mikkola, J. Power Sources 171 (2007) 26–36.
[11] H. Li, Y. Tang, Z. Wang, Z. Shi, S. Wu, D. Song, J. Zhang, K. Fatih, J. Zhang, H. Wang, Z. Liu, R. Abouatallah, A. Mazza, J. Power Sources 178 (2008) 103–117.
[12] H. Dohle, R. Jung, N. Kimiaie, J. Mergel, M. Müller, J. Power Sources 124 (2003) 371–384.
[13] H. Ju, C.-Y. Wang, S. Cleghorn, U. Beuscher, J. Electrochem. Soc. 153 (2006) A249–A254.
[14] G.-G. Park, Y.-J. Sohn, T.-H. Yang, Y.-G. Yoon, W.-Y. Lee, C.-S. Kim, J. Power Sources 131 (2004) 182–187.
[15] U. Pasaogullari, C.-Y. Wang, Electrochim. Acta 49 (2004) 4359–4369.
[16] Z. Qi, A. Kaufman, J. Power Sources 109 (2002) 38–46.
[17] D. Spernjak, A.K. Prasad, S.G. Advani, J. Power Sources 170 (2007) 334–344.
[18] S. Kim, B.K. Ahn, M.M. Mench, J. Power Sources 179 (2008) 140–146.
[19] S. Kim, M. Khandelwal, C. Chacko, M.M. Mench, J. Electrochem. Soc. 156 (2009) B99–B108.
[20] S. Kim, M.M. Mench, J. Power Sources 174 (2007) 206–220.
[21] R. Makharia, M.F. Mathias, D.R. Baker, J. Electrochem. Soc. 152 (2005) A970–A977.
[22] J. Kleemann, F. Finsterwalder, W. Tillmetz, J. Power Sources 190 (2009) 92–102.
[23] X.L. Wang, H.M. Zhang, J.L. Zhang, H.F. Xu, Z.Q. Tian, J. Chen, H.X. Zhong, Y.M. Liang, B.L. Yi, Electrochim. Acta 51 (2006) 4909–4915.
[24] J. Zhang, G. Yin, Z. Wang, Y. Shao, J. Power Sources 160 (2006) 1035–1040.
[25] F. Podczeck, Particle–Particle Adhesion in Pharmaceutical Power Handling, Imperial College Press, London, 1998.
[26] C. Lamb, M. Zecchino, Wyko Surface Profilers Technical Reference Manual, Veeco Metrology Group, 1999.
[27] R. Chopra, F. Podczeck, J.M. Newton, G. Alderborn, Part. Part. Syst. Char. 19 (2002) 277–283.
[28] Balzers Sputter Coater SCD 050—Operating Instructions, 1990.
[29] D. Faith, C.J. Horsfield, J. Mater. Sci. 41 (2006) 3973–3977.
[30] S. Dallaire, M. Dufour, B. Gauthier, J. Therm. Spray Technol. 2 (1993) 363–368.
[31] J.E. Dove, J.D. Frost, Geosynth. Int. 3 (1996) 369–392.
[32] A. Bevilacqua, A. Gherardi, 1st International Workshops on Image Processing Theory Tools and Applications, 2008.
[33] M.D. Abramoff, P.J. Magelhaes, S.J. Ram, J. Biophoton. Int. 11 (2004) 36–42.
[34] D. Bessarabov, R. Sanderson, J. Membr. Sci. 244 (2004) 69–76.
[35] S.F. Timashev, D.G. Bessarabov, R.D. Sanderson, S. Marais, S.G. Lakeev, J. Membr. Sci. 170 (2000) 191–203.
[36] British Standard 1134, Method for the Assesment of Surface Texture, British Standard Institution, 1972.
[37] T. Swamy, E.C. Kumbur, M.M. Mench, J. Electrochem. Soc. 157 (2010) B77–B85.
[38] G. Lin, T.V. Nguyen, J. Electrochem. Soc. 153 (2006) A372–A382.
[39] A.Z. Weber, J. Newman, J. Electrochem. Soc. 152 (2005) A677–A688.
[40] J.T. Gostick, M.A. Ioannidis, M.W. Fowler, M.D. Pritzker, Electrochem. Commun. 11 (2009) 576–579.
[41] A. Turhan, S. Kim, M. Hatzell, M.M. Mench, Electrochim. Acta. (in press), doi:10.1016/j.electacta.2009.11.095.
[42] C. Hartnig, I. Manke, R. Kuhn, N. Kardjilov, J. Banhart, W. Lehnert, Appl. Phys. Lett. 92 (2008).
[43] J.H. Nam, K.-J. Lee, G.-S. Hwang, C.-J. Kim, M. Kaviany, Int. J. Heat Mass Transf. 52 (2009) 2779–2791.
[44] M.P. Manahan, S. Kim, E.C. Kumbur, M.M. Mench, ECS Trans. 25 (1) (2009) 1745–1754.
[45] Sigracet diffusion media, manufacture data sheet, Web: http://www.sglcarbon.com/sgl.t/fuelcell/index.html.